Egypt. J. Soil Sci. **Vol. 65,** No. 3, pp: 1383 - 1403 (2025)

Egyptian Journal of Soil Science
http://ejss.journals.ekb.eg/

Quantifying Soil Organic Carbon in Arid Ecosystem Using Geospatial Tools: A Case Study of Protected Areas in Bahawalpur district, Punjab, Pakistan

Muneeb Khalid, Sangam Khalil, Muhammad Abid, Tanveer Hussain, Muhammad Rafay and **Muhammad Madnee**

Institute of Forest Sciences, The Islamia University of Bahawalpur, Bahawalpur 63100, Pakistan

SPATIAL interpolation with mapping is crucial for estimating the soil carbon pool under changing land use pattern. Different land uses have effect differentially on carbon pool in in different ecosystems. The soil organic carbon (SOC) was predicted by using Inverse distance weighting (IDW) and ordinary kriging (OK). For this Circular 200 plot samples were taken (0.1 ha or 17.84 m radius). Study area was stratified on the basis of Land use i.e Forests, Range Lands, Barren Lands, sand dunes and water bodies. Landsat 8,9 images were downloaded from USGS Earth Explorer website. The pre-processing of the Landsat images for making maps of biomass was done in ENVI 5.3/SNAP 3.0. The processed images were analyzed and vegetation indices were computed. Statistical relationship was established with computed indices and departmental data. Total carbon of LSNP was calculated 21.51 m^3/m^2 while the total carbon stock from Cholistan wildlife sanctuary was 39.9gm/m^2. Spatial distribution of biomass of LSNP indicated, the biomass is influenced by tree age, as young trees tend to have lower biomass, whereas old trees have higher biomass due to their age-related growth patterns. The spatial distribution of the IDW interpolation appears to align with the SLR model. MLR model illustrates elevated SOC levels (1.0 to 1.20) in the southern regions, whereas a decline in SOC content (0.56 to 0.77) was noticeable in the northern parts of the study area. However, SOC levels near water bodies exhibited higher values, likely attributable to the presence of sparse vegetation. Conclusively this study provides basic information for establishment of carbon sink centers to combat adverse impacts of global warming, and climate change.

Keyword: LSNP, SOC, Vegetation indices, OK, Land use pattern.

1. Introduction

The world's largest organic carbon store is thought to be found in soil. It makes up around 75% of the terrestrial ecosystem's TC (Total Carbon) pool. Where flora and atmosphere and soil reserve 620 pg and 780 pg and soil stores 1500–1600 pg C respectively (Jobbagy and Jackson, 2000; Chung *et al*., 2008; Greve *et al*., 2009; Luo *et al*., 2010; Elbasiouny *et al*., 2014). One of the key elements of soil health and quality is SOC (Gregorich *et al*., 1994) that is crucial agricultural production (Stevenson and Cole, 1999). Soil structure, ability to store water, and cation-exchange capabilities are important factors that affect soil fertility. Additionally, it is crucial to the humification process of soil organic matter (SOM) (USDA-NRCS, 1995). Evaluating SOC stock using point location data is challenging. We can measure the location points of SOC which can be used to estimate the SOC stock by using spatial interpolation techniques and taking into account numerous factors impacting SOC (Gogoi *et al.*, 2024).

Human activity drives the broad, important processes of land use/cover dynamics, which also result in changes that ultimately affect the human life. Anthropogenic activities have been the cause of the decline in forest cover over the past few decades, which caused a global environmental problem. Four processes need to be taken into account when identifying natural resources, identifying changes that have happened, categorizing environmental changes, and figuring out the degree and patterns of change. In the past few decades, there have also been significant changes in land cover and use, such as the clearance of forest regions to make way for infrastructure, agricultural, engineering projects, and barren places. Land use land cover (LULC) mapping is important for the fulfillment of the objectives regarding management of the land, ecological research and to make available the proper information on suitable planning and management of natural resources (Sahu and Ghosh, 2021; Gogoi *et al.*, 2024).

The SOC spatial variability is an important method for the measurement of the soil quality and carbon pools in terrestrial ecosystem and also essential for the forecasting of environment, ecological modeling, agriculture and also for Natural resource management (Zhang *et al*., 2012; Liu *et al*., 2014; Wei *et al*., 2008). The characteristics

*Corresponding author e-mail: m.abid@iub.edu.pk
Received: 01/05/2025; Accepted: 15/07/2025
DOI: 10.21608/ejss.2025.380697.2149

of the SOC geographic distribution will be made available to the public, assisting in the establishment of the framework for evaluating soil fertility and supporting the development of reasonable agricultural environmental management plans. Scientific management is essential for SOC nutrients to grow in agricultural systems in a sustainable manner. As a result, adequate information about the spatiotemporal behavior of SOC over a region is needed. On the other hand, SOC measurements are expensive and time-consuming by nature, particularly if a soil sample is needed for installation (Kingsley *et al.*, 2021).

Many statistical and geostatistical methods have been used in the past to determine the spatial distribution of SOC (Kumar *et al*., 2012, 2013; Kingsley *et al.*, 2021). Using classical statistics, it was unable to determine the geographical distribution of soil characteristics at the un-sampled regions. Geo-statistics is a useful tool for examining the spatial distribution of soil qualities and their variability, as well as for reducing execution costs and assessment error variance (Saito *et al*., 2005; Liu *et al*., 2014; Behera and Shukla, 2015; Kingsley *et al.*, 2021).

Geospatial approaches were also used for the evaluation of soil spatial relationships and also for the amount by which properties of soil can fluctuate (Wei *et al*., 2008; Zhu *et al*., 2022). For the prediction of spatial distribution of the properties of soil, the ordinary kriging (OK) proved much valuable than inverse distance weighting (IDW) method (Zare-mehrjardi *et al*., 2010; Raheem *et al*., 2023). Robinson and Metternicht, (2006) described three divergent methodologies were used for the prediction of SOC. These methodologies included ordinary kriging and inverse distance weighting. The kriging method which is mostly used in recent researches is OK (ordinary kriging) through which estimates of surface maps of soil properties can be produce (Pang *et al*., 2011). For the spatial prediction of TSD (total dissolved solids) in water used for drinking, the most operational technique is EBK (Empirical Bayes kriging) (Hussain *et al*., 2014; Patel *et al.*, 2024) and this technique also performed better as compare to other geo-statistical methods i.e ordinary kriging (OK) and inverse distance weighting (IDW) for the assessment of contamination in ground water (Mirzaei and Sakizadeh, 2015; Zhu *et al*., 2022).

Despite these advancements, there remains a noticeable research gap in spatial SOC modeling within arid and semi-arid ecosystems like the Cholistan Desert-especially under varied land use patterns such as forests, rangelands, barren lands, and sand dunes. Few studies have comprehensively evaluated the comparative efficiency of interpolation methods like OK and IDW in such harsh, ecologically sensitive environments (Robinson and Metternicht, 2006; Zare-mehrjardi *et al*., 2010; Patel *et al*., 2024). Furthermore, the integration of remote sensing-derived vegetation indices with ground-based carbon estimates is underexplored in these regions. To address this gap, this study investigates the spatial distribution of SOC using geospatial interpolation methods in Lal Suhanra National Park (LSNP) and Cholistan Wildlife Sanctuary (CWLS), integrating remote sensing data, vegetation indices, and field sampling. The objective is to determine the most suitable interpolation technique for SOC prediction in the study area and provide foundational data for the development of carbon sink centers for land managers and policy makers to mitigate the impacts of climate change.

2. Materials and Methods

2.1. Study Area

This research was carried out in the Protected Areas (Lal Suhanra National park and Cholistan Wildlife Sanctuary) of Bahawalpur District.

Lal Suhanra National Park: Lal Suhanra National Park (LSNP) having an area of 162567 acres (Survey Punjab Wildlife and Parks Department 2022) is located between 29° 12' and 29° 28′ northern latitude and 71° 48′ and 72° 08′ eastern longitudes, with an altitude from 125 to 140m. The area is highly diversified by flora and fauna, three different microhabitats and cultural heritage, to conserve these resources the area was notified as national park in 1972. LSNP is of monstrous worth because of irrigated plantation, enclosures of wildlife, recreation facilities as well as fishing in the lake. The changing soil physio-chemical characteristics, the area assumes a significant part in conserving biodiversity of the area. Vegetation is generally sparse whereas desert region upholds the xeric and semi-xeric sort of vegetation. The Lake has the hydrophytes and mesophytes (Wariss *et al*., 2014).

Cholistan Wildlife Sanctuary: The Cholistan desert is a section of the world's seventh biggest desert, the Great Desert, which is extended along the south line of Punjab area, Pakistan. The area of the Cholistan desert is 660,921 ha; it is situated 29º 59' North as well as 73º 16' East at an altitude of around 112m (Abid *et al*., 2024). Geography, soil type and surface, along with plantation structure separate this desert into two specific areas: the northern locale (Lesser Cholistan) covers around 7,770 km^2 as well as the southern area (Greater Cholistan) around 18,130 km^2 (Guidelines for sensitive and critical areas, Govt. of Pakistan, Oct 1997).

Soil and Climate: Due to insignificant amount of organic matter, the soil of Cholistan desert is considered as poor. The Lesser Cholistan is described by huge saline compacted with alluvial soil (inter-dunal flats), which are generally stabilized to semi-stabilized. Soil of interdunal sites differs in surface, structure, and the degree of salinity and sodicity with pH ranges from 8.2 to 9.6. Sand dunes are much lower (under 100 meters) than those found in Greater part. The Greater Cholistan is involved by hot desiccated winds that lead to sand dune shifting even a huge sand dune can be converted into Interdunal surface. Cholistan desert is severe dry and long summer droughts which may extend for 4-6 years consistently. Mean summer temperature varies from 35-50 ºC during May to June as well as winter from 12-15 ºC December to February. Annual precipitation is low and inconsistent, annual rainfall ranging from 100-200mm/year mm with its maximum during July to September during monsoons and January to March during winters (Hameed *et al*., 2011; Abid *et al*., 2024).

2.2. Data collection and analysis

Stratification of the area

Study area was stratified on the basis of Land use classes in both sites i.e Forests, Range Lands, Barren Lands, sand dunes and water bodies, for Lal Sohanra national park (Forest types i.e Thorn forests/Irrigated forests). Data collection from Cholistan wildlife sanctuary was also based on geographic distribution Range lands, Barren lands, water bodies, sand dunes and irrigated lands.

Field Sampling and Estimation of Carbon Stocks

Circular plots of 0.1 ha (17.84 m radius) were randomly established in stratified land cover classes. Tree species data (DBH and height) were recorded, and above-ground biomass (AGB) was calculated using species-specific allometric models and biomass expansion factors (BEF). AGB was converted to carbon using the IPCC-recommended coefficient of 0.47. Below-ground biomass (BGB) was estimated using a root-to-shoot ratio (R/S = 0.26).

Soil samples were taken at depths of 0–15 cm and 15–30 cm from each plot, and SOC was measured via laboratory analysis. Bulk density was calculated from dried soil cores.

Above Ground Biomass (AGB) for tree species

The data were collected from both sites by using random sampling. Tree height was measured by using wooden protector, Diameter was taken at diameter at breast height (DBH 4.5 feet) and converted into volume. (Ekoungoulou *et al*., 2015).

Data analysis in three (03) pools:

Above Ground Biomass (AGB)

Above ground biomass was calculated from the stem biomass and biomass expansion factor. Stem biomass was calculated from the volume (m^3) and wood density of the tree species. (Ahmad *et al*., 2014), Table 1a.

$$\text{Stem biomass} = \text{Volume} \times \text{Wood density}$$

For the calculation of total above ground biomass, Biomass Expansion Factor (BEF) was used which was established for each species.

$$AGB = V \times WD \times BEF$$

Whereas:

AGB= Above Ground Biomass

V= Volume

WD= Wood Density

BEF= Biomass Expansion Factor

BEF= Total AGB^w/BM^b

Whereas,

AGB^w= Above ground biomass of a whole tree (limbs, branches, twigs & leaves)

BM^b= Biomass of a tree bole till merchantable height (Ali *et al*., 2020)

Table 1a. Showing the Expansion factor of different species for the estimation of total Above Ground Biomass.

Sr. no.	Species name	Biomass Expansion factor (BEF= AGB^w/BM^b)
1	*Vachillia nilotica*	1.2
2	*Tamarix aphylla*	1.2
3	*Prosopis cineraria*	1.4
4	*P. glandulus*	1.7
5	*P. juliflora*	1.4
6	*Salvadora oleoides*	1.2
7	*S. persica*	1.3
8	*Ziziphus jujuba*	1.5
9	*Z. mauritiana*	1.12
10	*Z. spine cristi*	1.5
11	*Z. nummularia*	1.5

The estimation of total carbon from biomass was done by multiplying the obtained above ground biomass with conversion factor which determine the average carbon in biomass. So, the co-efficient of 0.47 was used for the conversion of biomass to carbon.

Total carbon= 0.47 x Biomass

The co-efficient is widely used internationally; therefore, it has been applied in current research for the estimation of total carbon in above ground biomass (Vicharnakorn *et al*., 2014).

Pool 2: Below Ground Biomass (BGB)

To calculate below ground biomass of BGB= AGB x R/S

Whereas:

BGB= Below Ground Biomass

AGB= Above Ground Biomass

R/S Ratio= Root-Shoot Ratio (0.26) (Kumar *et al*., 2022; IPCC, 2003; Grass Biomass Production, 2023).

Pool 3: Soil Carbon

Soil samples were collected at 0-15 and 15-30cm soil depth from each plot by using an Augar (Nizami *et al*., 2009). Soil samples of top soil were also collected from each plot. Fresh weight of each sample was measured by using weighing machine. Samples were air dried in the laboratory and weight was measured again by using electrical balance. Soil carbon, above and below ground soil carbon was measured by using the following methodology.

$$SOC = BD \times D \times \%C$$

Whereas:

SOC = Soil Organic Carbon Stock

BD= Soil Bulk Density

D= the total depth at which the sample was taken.

% C = Carbon concentration (%) amounting to 0.47 of biomass or taken from lab measurements

Bulk density of the soil = Dry weight of the soil/Volume of the core (Ali *et al*., 2020; Magar *et al*., 2020)

2.3. Integration of Field Sampling with Remote Sensing Data

To ensure robust spatial estimation of biomass and soil organic carbon (SOC), remote sensing data were integrated with ground-based field sampling. This process involved image pre-processing, spectral index computation, and statistical validation against field data.

Landsat 8 and 9 Level-1 data were downloaded from the USGS Earth Explorer portal for the time period corresponding as closely as possible to field data collection. Preprocessing was conducted using **ENVI 5.3 and SNAP 3.0**, and included the following steps:

- **Radiometric Calibration**: Conversion of digital numbers (DN) to Top-of-Atmosphere (TOA) reflectance.
- **Atmospheric Correction**: Performed using the FLAASH module to reduce atmospheric interference.
- **Georeferencing and Reprojection**: All scenes were corrected to WGS 84, UTM Zone 42N.
- **Cloud and Shadow Masking**: Implemented using the Fmask algorithm to exclude cloud-covered pixels.
- **Image Subsetting**: Study areas (LSNP and CWLS) were extracted using vector shapefiles for region-of-interest (ROI) analysis.

The processed images was then analyzed and computation of vegetation indices was done to find forest density and biomass. Indices were computed using raster calculator tools in ENVI and exported as georeferenced layers for spatial analysis. After image processing, statistical relationship was established with computed indices and departmental data. The forest attributes (vegetation indices and biomass) was analyzed against explanatory variables.

2.4. Model Calibration and Validation

Field-estimated biomass and SOC values were statistically correlated with the spectral indices using:

- Simple and multiple linear regression (SLR and MLR).
- Stepwise regression to identify the most significant predictors.
- Models were evaluated using coefficient of determination (R^2), root mean square error (RMSE), and standard error of the estimate (SEE).

To ensure accuracy and generalizability 70% of field data were used for model calibration and 30% for independent validation. Performance was assessed by comparing predicted vs. observed values using validation metrics (R^2, RMSE, MAE). Residual plots and scatterplots were used to visualize model fit.

2.5. Spatial Mapping

The best-performing regression models were applied to the full spectral index Rasters using ArcGIS 10.3 to generate biomass and SOC spatial distribution maps. For interpolation of soil carbon, both Inverse Distance Weighting (IDW) and Ordinary Kriging (OK) were used, and their performance compared.

1. Landsat-8, 9 product acquisition from https://earthexplorer.usgs.gov/, for nearest possible time when forest inventory was done.
2. Landsat-8 product acquisition from https://earthexplorer.usgs.gov/, for the current forest inventory time.
3. Image classification of both images for land use changed detection (Margono *et al.,* 2012).

2.6. Interpolation methods

The present study used both geostatistical i.e., using the statistical qualities of the measured points and deterministic i.e., creating surfaces from measured point's interpolation approaches. The spatial distribution of SOC was generated in this study using a range of deterministic interpolation techniques, such as those based on the degree of smoothing (radial basis functions), the extent of similarity (inverse distance weighted), local polynomial interpolation (LPI), or geostatistical interpolation, namely ordinary kriging (OK) and Empirical Bayes (EBK) (Johnston *et al*., 2001). Only inverse distance weighting and ordinary kriging method was used for mapping.

2.7. Inverse Distance Weighting (IDW)

In the field of soil research, one of the most widely used deterministic interpolation methods is the IDW. IDW calculations were based on recognized places that were close by. The inverse of the distance from the interpolation point determines the weights applied to the interpolating points. As a result, the close points are weighted more than the distant points, and vice versa, meaning that they have greater impact. It is implicit that the known sample points are independent of one another (Robinson and Metternicht, 2006).

$$Z(X_0) = \Sigma^{n}_{i=1} x_i / h^{\square}_{ij} / \Sigma^{n}_{i=1} 1/h^{\square}_{ij}$$

Where ß indicates the weighting power, xi is the ith data value, ij is the separation distance between the interpolated value and the sample data value, and z(x0) is the interpolated value. The total number of sample data values is represented by n.

2.8. Ordinary kriging (OK)

The statistical characteristics of the observed data (spatial autocorrelation) are incorporated into the ordinary kriging approach. By using the semi-variogram, the kriging approach expresses the spatial continuity

(autocorrelation). The statistical correlation's strength as a function of distance is determined by the semi-variogram. The sill corresponds to the maximal variability in the absence of geographical dependence, and the range is the distance at which the spatial connection disappears. The goodness of fit was assessed using the coefficient of determination (R2) (Robertson, 2008).

Kriging estimate $z^*(x_0)$ and error estimation variance $\sigma k^2(x_0)$ at any point x_0 were, respectively, calculated as follows:

$$Z^*(X_0) = \Sigma^n_{i=1} \lambda_i z(x_i)$$

$$\sigma^2 k(X_0) = \mu + \Sigma^n_{i=1} \lambda_i \gamma(x_0 - x_i)$$

Where λi are the weights; μ is the lagrange constant; and γ (x0 _ xi) is the semi-variogram value corresponding to the distance between x0 and xi (Vauclin *et al*., 1983; Agrawal *et al*., 1995).

2.9. Statistical Analyses

A spectral index includes normalized difference vegetation Index (Rouse *et al*., 1973), Soil Adjusted Vegetation Index (SAVI) (Qi *et al*., 1994), Difference Vegetation Index (DVI) (Jordan, 1969), Modified Soil Adjusted Vegetation Index (MSAVI) (Qi *et al*., 1994), Perpendicular Vegetation Index (PVI) (Perry and Lutenschlager, 1984), Brightness index (BI) (Mondal *et al*., 2017), Redness index (RI), Colour index (CI), Vegetation (Veg) Second brightness index (BI2) (Gholizadeh *et al.*, 2018), Shortwave infrared (SWIR), Second shortwave infrared (SWIR2) (Nield *et al*., 2007), Normalized Difference Spectral Indices (NDSI) (Boschetti *et al*., 2014). Regression model for the mapping of biomass spatial distribution in carbon stock will be developed all over the research area. OK (ordinary kriging) and IDW (Inverse distance weighting) was used for interpolation (Addis *et al*., 2016).

3. Results

3.1. Soil organic carbon of LSNP and CWLS

Table 1b shows the significant results above ground biomass of different tree species in Cholistan wildlife sanctuary m^3/m^2 during two years of research (2021-2022). Total volume of *Vachellia nilotica* during 2021 was 3.28675 m^3 and during 2022 was 0.97541 m^3, for *Tamarix aphylla* during 2021 was 9.81100 m^3 and during 2022 was 5.79375 m^3. Soil organic carbon are shown in table 1b.

Table 1b. Year wise mean values of volume, Above ground biomass (AGB), Below ground biomass (BGB), Total biomass (TB) and Total carbon of selected tree species in Cholistan wildlife sanctuary.

Species	Years	Tree volume (m^3)	AGB M^3/m^2	BGB M^3/m^2	TB M^3/m^2	TOTAL CARBON M^3/m^2
Vachellia nilotica	2021	3.28675	0.006705	0.001743	0.00844	0.003971
	2022	0.97541	0.001756	0.000456	0.00221	0.001039
Tamarix aphylla	2021	9.81100	0.012951	0.003367	0.01631	0.007669
	2022	5.79375	0.006257	0.001626	0.00788	0.003705
Prosopis cineraria	2021	1.02972	0.001009	0.000262	0.00127	0.000598
	2022	0.44640	0.000312	0.000038	0.00035	0.000164
P. glandulus	2021	0.16945	0.000432	0.000112	0.00054	0.000256
	2022	0.17711	0.000331	0.000060	0.00039	0.000184
P. juliflora	2021	0.62876	0.002201	0.000572	0.00277	0.001303
	2022	0.22715	0.000636	0.000165	0.00080	0.000376
Salvadora oleoides	2021	5.47202	0.00591	0.001536	0.00744	0.0035
	2022	5.43358	0.003912	0.001017	0.00493	0.002316
S. persica	2021	3.48357	0.001359	0.000353	0.00171	0.000805
	2022	0.19448	0.000075	0.000019	0.00010	0.000042
Ziziphus jujube	2021	0.27768	0.000458	0.000055	0.00051	0.000242
	2022	1.16419	0.001397	0.000363	0.00176	0.000827
Z. mauritiana	2021	17.3457	0.054396	0.014143	0.06853	0.032213
	2022	12.2024	0.030066	0.007817	0.03788	0.017805
Z. spine cristi	2021	3.96266	0.004161	0.001081	0.00524	0.002464
	2022	2.43291	0.002189	0.000569	0.00276	0.001296
Z. nummularia	2021	0.33023	0.000693	0.000180	0.00087	0.000411
	2022	0.24308	0.000401	0.000049	0.00045	0.000211

3.2. Biomass and carbon stock of desert and LSNP

Figure 1 explains that biomass gm/m^2 in desert (CWLS) is 175.83 and biomass m^3/m^2 in LSNP is 45.179. The carbon gm/m^2 in desert is 87.91 and carbon m^3/m^2 in LSNP is 21.514.

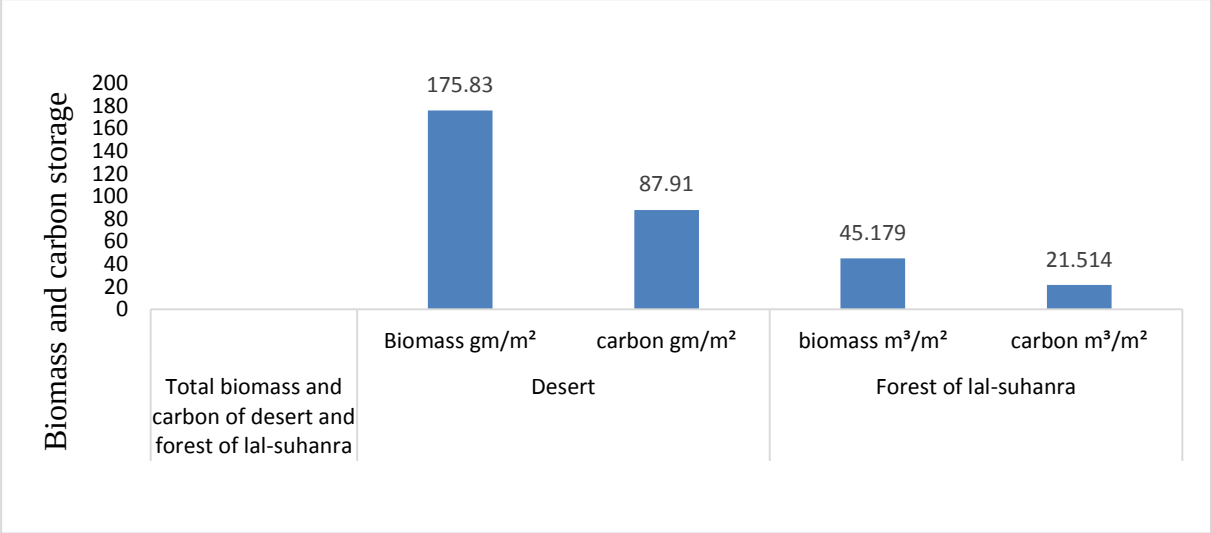

Fig. 1. Biomass and carbon stock of Cholistan wildlife sanctuary (CWLS) and Lal Suhanra national park (LSNP).

Table 2 describes the total amount of carbon in different depths of CWLS and LSNP during the year 2021. The results indicate that total carbon in rangelands of CWLS was 0.274942 g/m^2 in top soil, 0.330916 g/m^2 in 1-15cm and 0.323666 g/m^2 in 15-30cm. Maximum carbon is present in irrigated lands of CWLS as shown in table 2.

Table 3 describes the total amount of carbon in different depths of CWLS and LSNP during the year 2022. The results indicate that total carbon in rangelands of CWLS was 0.259571 g/m^2 in top soil, 0.323956 g/m^2.

Table 2. Mean values and standard error of soil carbon g/m^2 at different depths in CWLS and LSNP 2021.

Stratifications	CWLS (2021)			LSNP (2021)		
	Top soil	1-15cm	15-30cm	Top soil	1-15cm	15-30cm
Range lands	0.27±0.07	0.33±0.09	0.32±0.07	0.24±0.08	0.29±0.18	0.28±0.1
Barren lands	0.22±0.14	0.155±0.1	0.14±0.1	0.21±0.09	0.24±0.11	0.23±0.11
Sand dunes	0.32±0.059	0.37±0.078	0.33±0.07	0.20±0.13	0.21±0.12	0.22±0.11
Water bodies	0.268±0.16	0.19±0.08	0.22±0.19	0.25±0.09	0.21±0.09	0.28±0.07
Forest (LSNP), Irrigated lands (CWLS)	0.33±0.1	0.35±0.1	0.37± 0.1	0.22±0.09	0.27±0.13	0.28±0.1

Table 3. Mean values and standard error of soil carbon gm/m^2 at different depths in CWLS and LSNP 2022.

Stratifications	CWLS (2022)			LSNP (2022)		
	Top soil	1-15cm	15-30cm	Top soil	1-15cm	15-30cm
Range lands	0.26±0.07	0.32±0.07	0.32±0.07	0.23±0.07	0.27±0.06	0.31±0.06
Barren lands	0.22±0.01	0.25±0.01	0.28±0.09	0.24±0.09	0.27±0.08	0.3±0.08
Sand dunes	0.29±0.8	0.31±0.07	0.33±0.07	0.19±0.01	0.21±0.01	0.23±0.08
Water bodies	0.25±0.17	0.28±0.12	0.27±0.12	0.26±0.05	0.29±0.05	0.32±0.05
Forest, (LSNP), Irrigated lands (CWLS)	0.33±0.07	0.36±0.06	0.39±0.05	0.54±0.24	0.27±0.11	0.31±0.08

3.3. Vegetation Indices from Landsat-9 Image

Various vegetation indices were computed from Landsat-9 imagery, encompassing the Normalized Difference Vegetation Index (NDVI), Soil Adjusted Vegetation Index (SAVI), Modified SAVI, Difference Vegetation Index (DVI), and Perpendicular Vegetation Index (PVI) as depicted in Figure 2. The NDVI values ranged from 0 to 0.42, where positive values (0.42 or less) indicated the presence of vegetation cover, while values of 0 or less suggested the absence or sparse vegetation. Similarly, Figure 2 (B) and (C) illustrated that SAVI and MSAVI values varied from 0 to 0.63 and 0.45 to 1.09, respectively. Higher values in these indices were indicative of dense vegetation, while lower values denoted areas with little to no vegetation. Additionally, elevated values in DVI and PVI corresponded to tropical thorn forests, while lower values were associated with rangelands and barren lands. Overall, the analysis of all vegetation indices revealed that forest density was scattered throughout the LSNP. Particularly, higher forest density was observed in the central regions of the study area, gradually decreasing from south to north. In contrast, the extreme eastern and western parts of the study area exhibited sparse vegetation, mostly comprising rangelands as shown in figure 2.

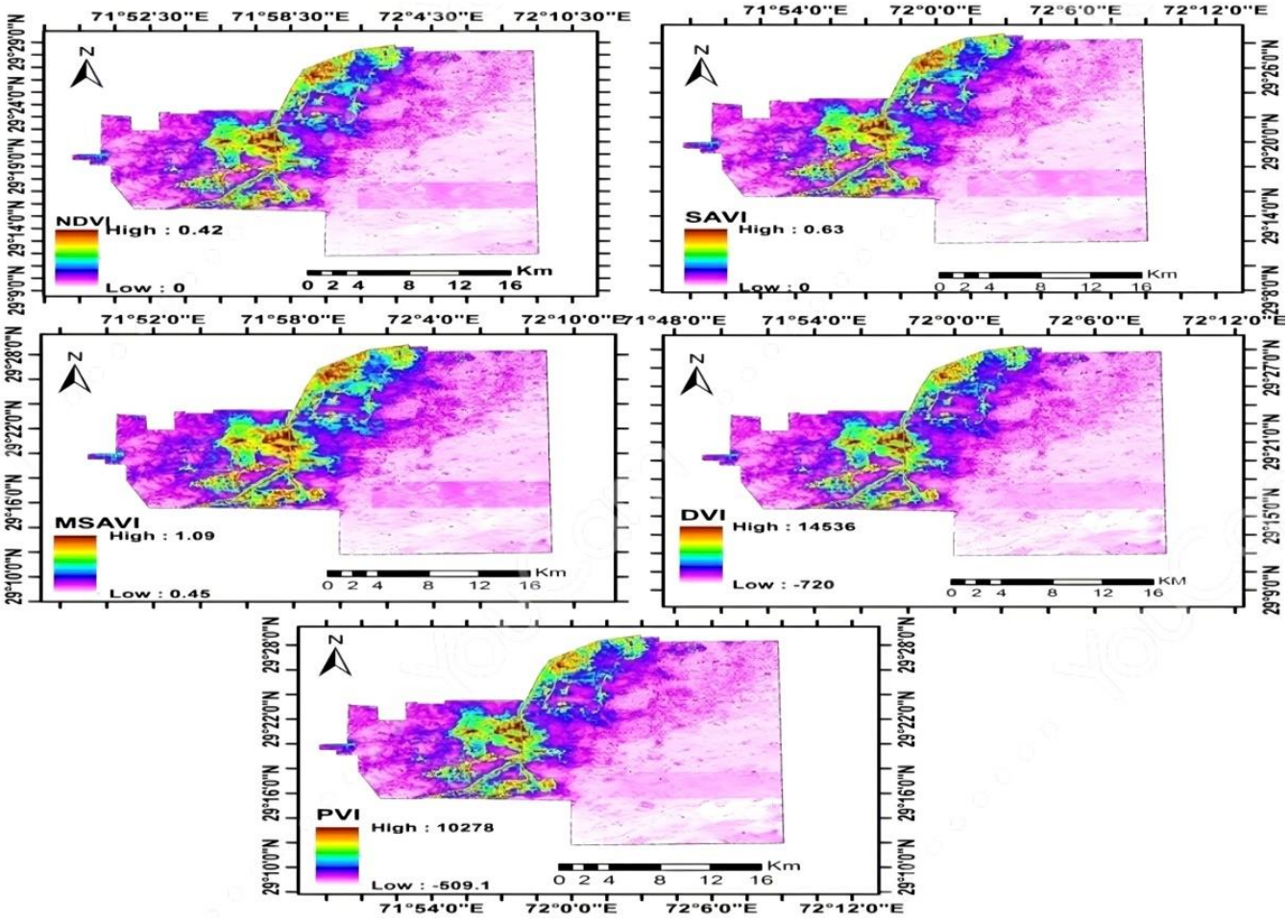

Fig. 2. Various vegetation indices were computed from Landsat-9 imagery, encompassing the Normalized Difference Vegetation Index (NDVI) (A), Soil Adjusted Vegetation Index (SAVI) (B), Modified SAVI (C), Difference Vegetation Index (DVI) (D), and Perpendicular Vegetation Index (PVI) (E).

3.4. Correlation between Biomass versus Landsat-8 Spectral Indices

The spectral indices included NDVI, SAVI, MSAVI, DVI, and PVI, while the other variables encompassed elevation, slope, aspect, mean annual temperature, and annual precipitation. Results indicated that all vegetation indices (NDVI, SAVI, MSAVI, DVI, and PVI) demonstrated a strong positive correlation with biomass (t/ha). Conversely, biomass displayed negative correlations with slope, aspect, mean annual temperature (MAT), and annual precipitation (APPT). Notably, the spectral indices DVI and PVI exhibited the highest correlation with biomass, achieving an R^2 value of 0.82. Following closely were NDVI and SAVI, showing an R^2 value of 0.80. MSAVI, on the other hand, demonstrated the lowest correlation among the spectral indices, with an R^2 value of 0.77. Regarding the other variables, such as elevation, aspect, slope, MAT, and APPT, their coefficient of correlation was deemed insignificant at the 0.05 and 0.01 significance levels (Figure 3).

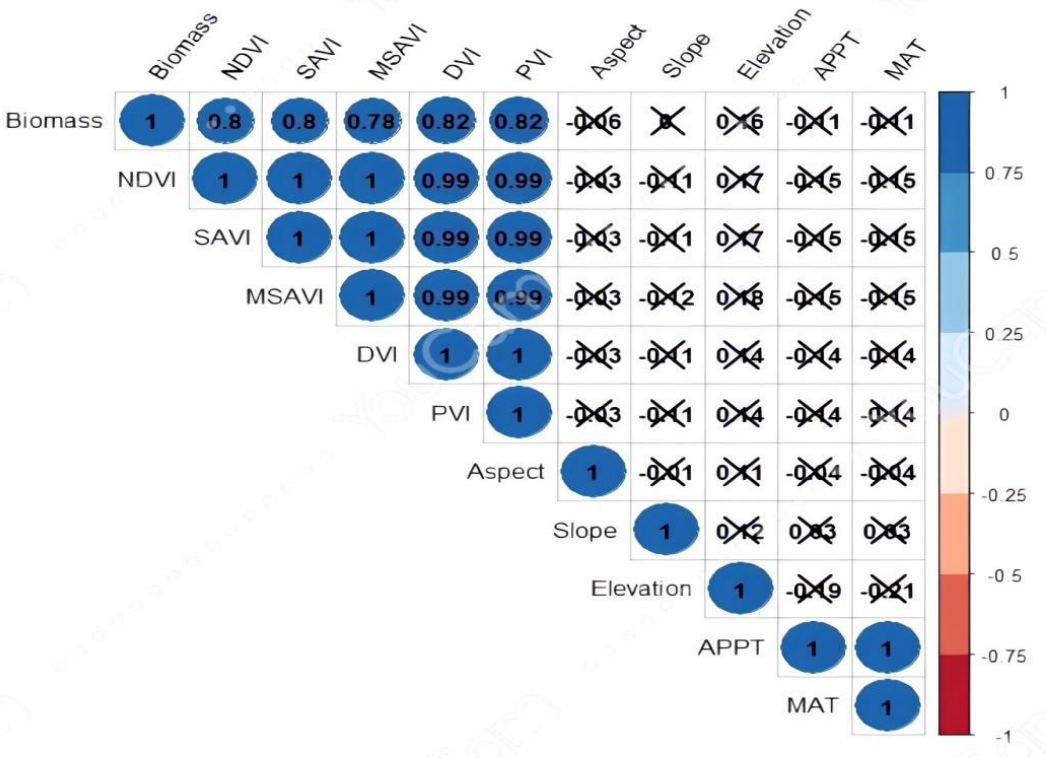

Fig. 3. A correlation matrix was created to examine the relationships between biomass (measured in t/ha) and various spectral indices derived from a Landsat-8 image, as well as topographic and climatic factors for variables (elevation, aspect, slope, MAT, and APPT).

3.5. Single Predictor Linear Regression between Biomass and Landsat-9 Spectral Indices

The results of single predictor linear regression models between biomass (t/ha) and spectral indices have been summarized in Table 4, while the corresponding scatterplots are displayed in Figure 4. The linear regression model using NDVI as a predictor showed a coefficient of correlation of 0.64. This means that approximately 64% of the field data was explained by the NDVI-based model, leaving around 36% of the data unexplained. Considering that NDVI is a proxy data, a correlation coefficient of this magnitude is considered good. Similar to NDVI, the regression model based on SAVI also exhibited a similar R^2 value, indicating that approximately the same proportion of variance (64%) in biomass data was explained by this index, leaving the remaining 36% unexplained. However, the coefficient of correlation for the MSAVI model (R^2 0.60) was lower than that of NDVI and SAVI, suggesting that this model explained around 60% of the biomass data, leaving 40% unexplained. In contrast, both DVI and PVI showed higher coefficient of correlation (R^2 0.67) compared to all other indices, indicating that they explained approximately 67% of the field biomass data, with about 33% remaining unexplained.

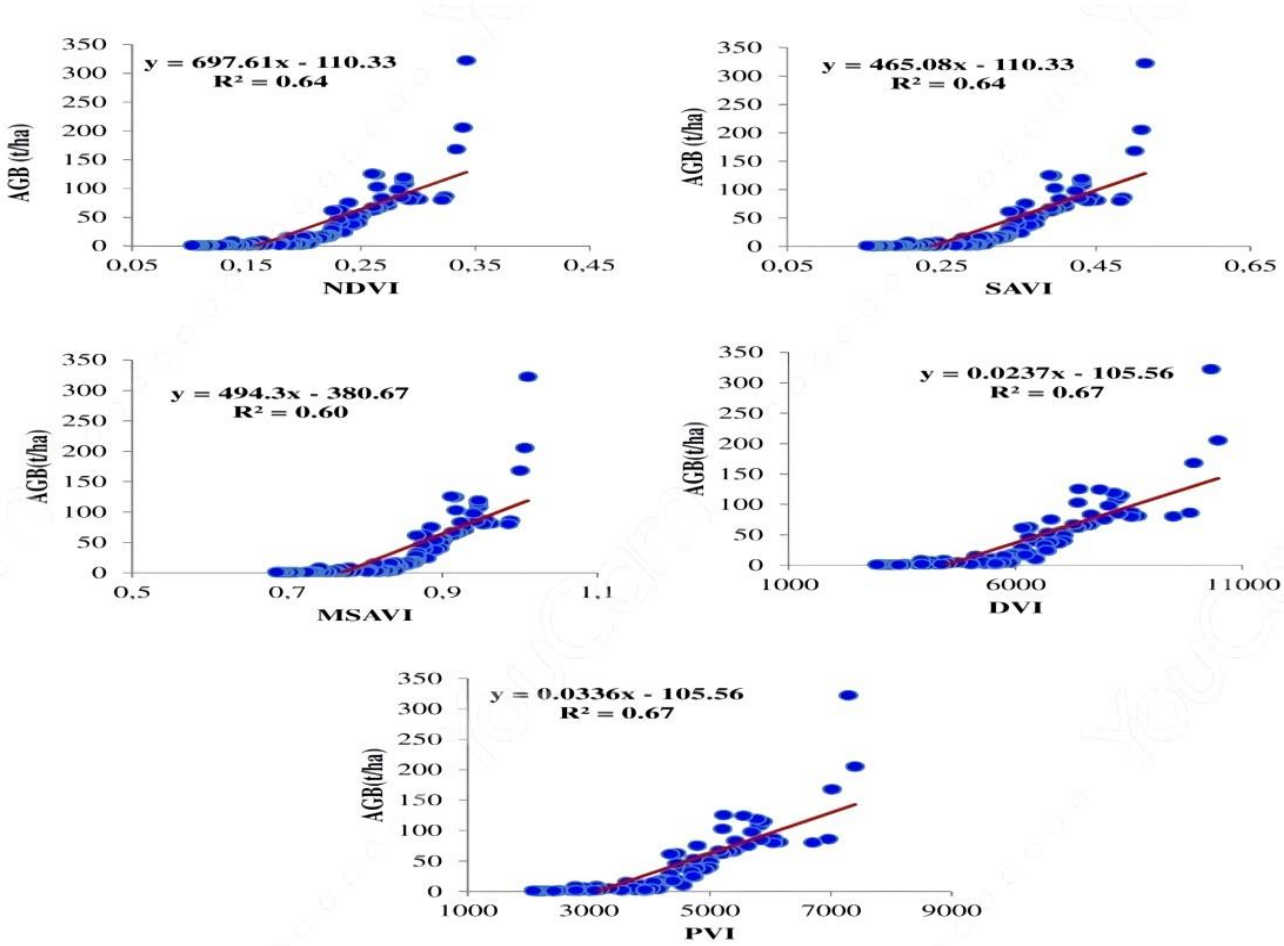

Fig. 4. Scatterplots of linear regression models b/w biomass and spectral indices Stepwise Linear Regression Model (SLRM).

Table 4. Single predictor linear regression models between biomass (t/ha) and spectral indices. Summary of regression models for Landsat-9 Spectral indices.

Indices	Equation	R^2	SE	F	P-value
NDVI	Biomass= 697.61*NDVI - 110.33	0.64	30.50	172.7	3.47E-23
SAVI	Biomass= 465.08*SAVI - 110.33	0.64	30.40	171.8	3.37E-23
MSAVI	Biomass= 494.3*MSAVI - 380.67	0.60	32.12	146.2	5.21E-21
DVI	Biomass = 0.0237*DVI - 105.56	0.67	29.12	198.72	4.07E-25
PVI	Biomass = 0.0336*PVI - 105.56	0.64	29.12	198.72	4.07E-25

3.6. Stepwise Linear Regression Model (SLRM)

The findings from the stepwise linear regression have been presented in Table 5. All spectral indices derived from Landsat-9 (NDVI, MSAVI, SAVI, DVI, PVI) were utilized as explanatory variables in the stepwise method. The final model selected the explanatory variables based on their significance levels, with a probability of being selected set to <= .050 and a probability for exclusion set to >= .100. As depicted in Table 3, the ultimate model indicated that MSAVI and SAVI were chosen as explanatory variables for biomass mapping in the study area. In contrast, the remaining indices (NDVI, DVI, and PVI) were not excluded from the model because their significance values exceeded the pre-defined threshold. The overall coefficient of determination for the model was 0.81, and the Adjusted R-squared was 0.812, with an error estimate of 22.01 (t/ha) for biomass.

Table 5. Stepwise Linear Regression Model and Biomass Mapping; a. Dependent variable: Biomass (t/ha); a. Predictors in the model: (Constant), MSAVI and SAVI; Stepwise (Criteria: Probability-of-F-to-enter <= .050, Probability-of-F-to-remove >= .100).

Variables entered/ removed			**Model summary**			
Variables Entered	Variables Removed	Significance	R	R Square	Adjusted R Square	Std. Error of the Estimate
MSAVI		.000	0.90	0.81	0.81	22.01
SAVI		.000	**ANOVA**			
	NDVI	.338		Sum of Squares	df	Mean Square
	PVI	.915	Regression	204044.5	2	102022.280
	DVI	.915	Residual	46044.5	95	484.679
			Total	250089.0	97	
Model Coefficients						
	Unstandardized coefficients		Standardized coefficients	T	Sig.	Model equation
	B	Std. Error	Beta			
(Constant)	2501.5	276.527		9.046	.000	Biomass = 2501.5 – 4692.8*MSAVI + 4737.4*SAVI
MSAVI	-4692.8	496.625	-7.377	-9.449	.000	
SAVI	4737.4	452.851	8.167	10.461	.000	

3.7. Spatial Distribution of Biomass in LSNP

The most optimal linear regression model was selected for spatial mapping based on its performance, primarily determined by the R^2 values. The resultant output, a spatial distribution biomass map, is presented in Figure 5. The predicted biomass from Landsat-9 data ranged from a minimum of 0 t/ha to 238 t/ha across the study area, as depicted in Figure 5. Analyzing the results, it becomes evident that the forest density is more pronounced in the central parts of the area, where tropical thorn forests extend from the southern to the northern regions. Conversely, the western and eastern sides exhibit lower vegetation or even barren and rangeland areas. Overall, the biomass of broadleaved species was observed to be lower, mainly due to reduced forest density and anthropogenic pressures. Furthermore, the biomass is influenced by tree age, as young trees tend to have lower biomass, whereas old trees have higher biomass due to their age-related growth patterns.

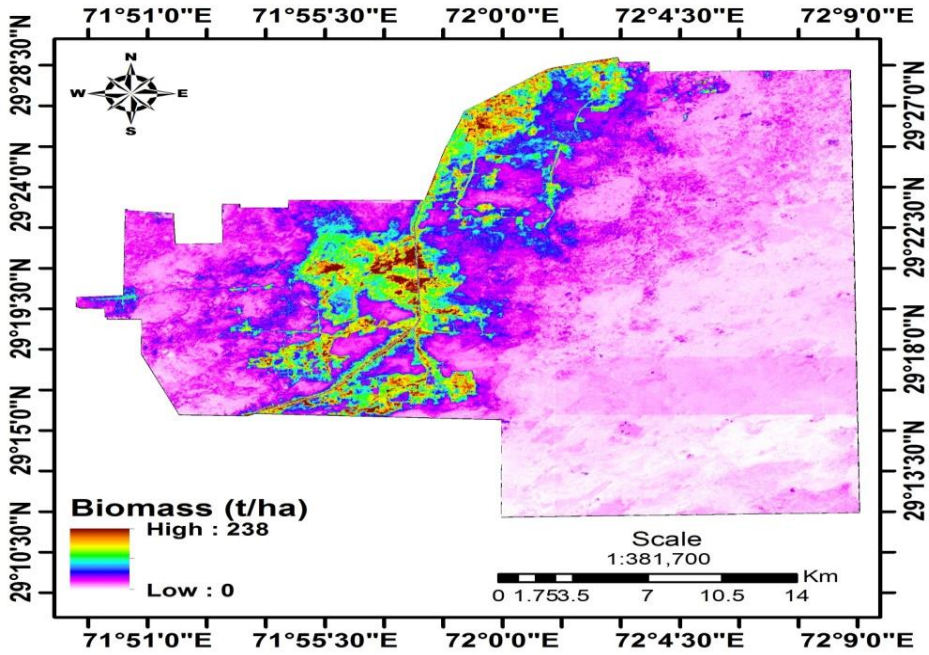

Fig. 5. Spatial Distribution of Biomass in LSNP; The most optimal linear regression model determined by the R^2 values .

3.8. Soil organic carbon of LSNP

Correlation between SOC and Landsat-9 Spectral Indices

The correlation results revealed that among all locations, SWIR/NIR exhibited the strongest correlation (R^2= 0.62) with Soil Organic Carbon (SOC), followed by BSI, SWIR2, and Veg, with correlations of 0.141, 0.137, and -0.136 respectively. Weaker correlations were observed between SOC and other indices (NDVI, SAVI, RI, CI, BI, BI2, SI, SOCI and NDSI). The relationship between SWIR and SOC proved to be highly significant at the 0.001 level, whereas the correlations of all other indices did not show significance. This analysis provided valuable insights that SWIR/NIR significantly influences the prediction of SOC using Landsat-8 data (table 6).

Stepwise Linear Regression Model between SOC and Spectral Indices

SLR model was developed to investigate the relationship between SOC and various explanatory variables, encompassing Landsat-9 spectral indices such as SWIR, Veg, RI, NDVI, SAVI, BI, RI, BI2, CI, SOCI, SI, BSI, and SWIR2. The SLR model adopted a stepwise approach for variable inclusion, considering significance values less than or equal to 0.50 as entry criteria, and removal probabilities equal to or exceeding 0.10, as displayed in Table 7. The outcomes of the SLR model demonstrated that out of the 13 explanatory variables, only three variables (SWIR, Veg, and RI) exhibited a significant relationship with SOC. Conversely, the remaining spectral indices were deemed insignificant and consequently excluded from the final model due to their p-values surpassing 0.10. The overall correlation of the SLR model was substantial, yielding an R^2 value of 0.45, which accounted for 45% of the variation in the SOC data, while 55% of the data remained unexplained. The adjusted R^2 stood at 0.43, accompanied by a standard error of 0.23. Furthermore, the model displayed proficient predictive capabilities, and the scatterplot depicting standardized predicted values against residuals. SLR model has three iterations and the coefficient of correlation has been increased from 0.387 (with 0.249 STD error) in the first model to the 0.452 (with 0.238 STD error) in the final model.

Table 6. Correlation between SOC and Landsat-9 Spectral Indices; **Correlation is significant at the 0.01 level (2-tailed).

	SOC	SAVI	NDVI	NDSI	SOCI	Veg	BSI	SWIR
SOC	1	-.124	-.124	.007	.046	-.136	.141	.622**
SAVI	-.124	1	1.000**	-.874**	-.919**	.998**	-.994**	.059
NDVI	-.124	1.00**	1	-.874**	-.919**	.998**	-.994**	.059
NDSI	.007	-.874**	-.874**	1	.982**	-.849**	.876**	-.085
SOCI	.046	-.919**	-.919**	.982**	1	-.901**	.921**	-.069
Veg	-.136	.998**	.998**	-.849**	-.901**	1	-.991**	.055
BSI	.141	-.994**	-.994**	.876**	.921**	-.991**	1	-.023
SWIR	.622**	.059	.059	-.085	-.069	.055	-.023	1

Table 7. Landsat-9 spectral indices such as SWIR, Veg, RI, NDVI, SAVI, BI, RI, BI2, CI, SOCI, SI, BSI, and SWIR2.

Stepwise Linear Regression for LSNP SOC 2022							
Variables entered/ removed			**Model summary**				
Entered	Removed	Sig	R	R^2	Adjusted R^2	Std. Error	
SWIR		.000	.673[c]	.452	.435	.238190	
Veg		.001	**ANOVA**				
RI		.014		Sum of Squares	df	Mean Square	F
	SAVI	.935	Regression	4.499	3	1.500	26.431
	NDVI	.935	Residual	5.447	96	.057	
	CI	.474	Total	9.945	99		
	BI2	.813	**Model Coefficients**				
	BI	.973		Unstandardized coefficients		Standardized coefficients	T
	NDSI	.769		B	Beta		
	SI	.535	(Constant)	-.896	.395		-2.268
	SOCI	.089	SWIR	1.187	.144	.625	8.260
	SWIR2	.951	Veg	-.500	.148	-.392	-3.375
	BSI	.886	RI	14459.258	5747.295	.292	2.516
Model equation; SOC = -0.896+1.187*SWIR-0.500*Veg+14459.2*RI Dependent variable: SOC Predictors in the model: (Constant), SWIR, Veg, RI Stepwise (Criteria: Probability-of-F-to-enter <= .050, Probability-of-F-to-remove >= .100).							

3.9. Spatial Mapping of SOC using SLR Model

The final model of the SLR model was utilized to create a spatial distribution of SOC across the study area using ArcGIS 10.3. The resultant SOC spatial map is presented in Figure 6, illustrating distinct patterns, which depicted elevated SOC levels in the southern regions, encompassing rangelands and barren lands, whereas a decline in SOC content was evident in the central parts of the study area. This reduction aligns with areas occupied by forests, plantations, and water bodies.

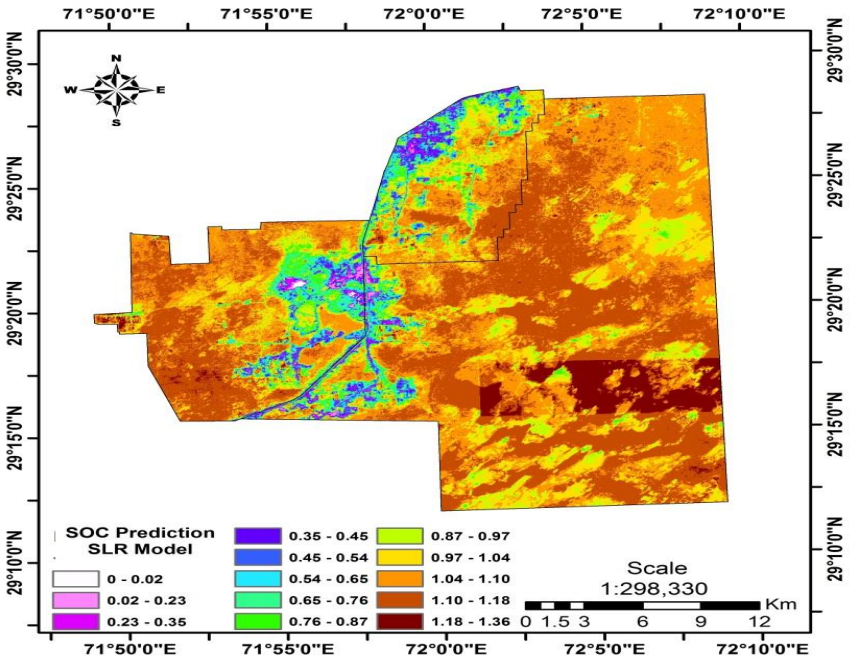

Fig. 6. SOC Prediction SLR Model; Final model of the SLR model was utilized to create a spatial distribution of SOC across the study area using ArcGIS 10.3.

3.10. SOC Interpolation by Inverse Distance Weightage Method

The Inverse Distance Weightage (IDW) technique was employed to generate a spatial interpolation of Soil Organic Carbon (SOC) across the study area, resulting in the map displayed in Figure 7. The findings indicated that the projected SOC values ranged from 0.14 to 1.04, with an average of 0.85. The standard deviation was 0.19, and the skewness coefficient was 0.49. Additionally, the kurtosis coefficient was calculated as 0.83 for the predicted SOC values. Analyzing the data distribution revealed a consistent pattern between observed and estimated SOC, with a standard error of 0.019. The spatial distribution of the IDW interpolation appears to align with the SLR model, particularly in the central section of the study area where forests, plantations and water bodies are situated.

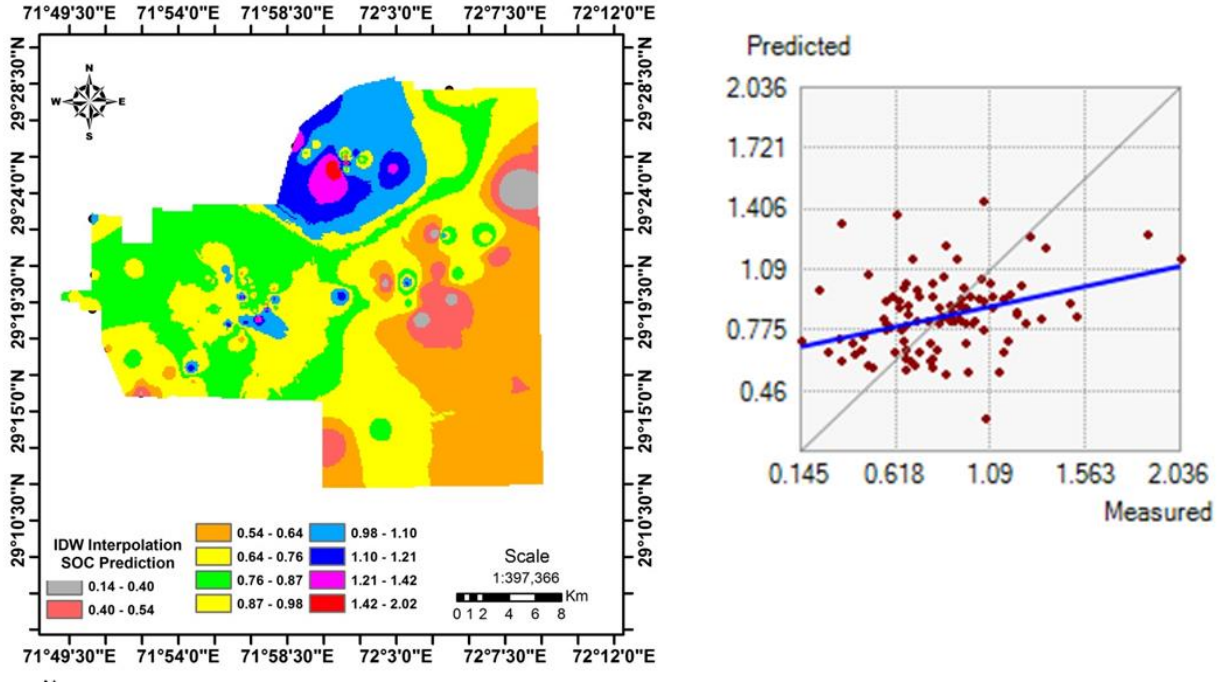

Fig. 7. IDW Interpolation SOC Prediction; The Inverse Distance Weightage (IDW) technique was employed to generate a spatial interpolation of Soil Organic Carbon (SOC) across the study area, resulting in the map.

3.11. Soil organic carbon of desert area

The results of correlation exhibited that among all locations, SAVI and NDVI showed the strongest correlation (R^2= 0.69) with SOC, followed by Veg SWIR and SWIR2 with correlations of 0.68, 0.61, and 0.56 respectively. Weaker correlations were observed between soil organic carbon and other indices (BSI, RI, CI, BI, BI2, SI, SOCI and NDSI). The relationship between BSI and SOC proved to be highly significant at the 0.01 level, while the correlations of all other indices did not show significance. This analysis provided valuable insights that SAVI and NDVI significantly influences the prediction of SOC using Landsat-9 data (table 8).

Multiple Linear Regression of Desert SOC and Spectral Indices

MLR model was developed using desert field-measured Soil Organic Carbon (SOC) as the dependent variable and various explanatory variables, including Landsat-9 spectral indices such as BI, RI, SAVI, SWIR2 BI2, CI, SOCI, SI, BSI, SWIR, Veg, RI, and NDVI. The MLR model followed an iterative approach for variable selection, where significance values equal to or less than 0.50 served as entry criteria, and removal probabilities exceeding or equal to 0.10 were considered, as detailed in Table 9. The output of the MLR model revealed that 08 explanatory variables, including Veg, SI, BSI, CI, SWIR2, SOCI, SWIR, and RI, were selected and included due to their significant relationships with SOC. Conversely, the remaining predictor variables were removed due to their weak association with field SOC. The overall correlation of the MLR model resulted in an R^2 value of 0.30, explaining only 30% of the variation in the SOC data, leaving 70% of the SOC data unexplained. The adjusted R^2 stood at 0.233, with a standard error of 0.25. The performance of spectral indices may be improved with high resolution satellite images and intensive field sampling.

Table 8. Correlations of soil organic carbon of desert area; correlation exhibited that among all locations, SAVI and NDVI showed the strongest correlation (R^2= 0.69) with SOC.

	SOC	BSI	SAVI	NDVI	NDSI	SOCI	SWIR	SWIR2	Veg
SOC	1	.493**	.069	.069	-.117	-.114	.061	.056	.068
BSI	.493**	1	.031	.031	-.285**	-.333**	.243*	.231*	.027
SAVI	.069	.031	1	1.000**	.148	.157	-.731**	-.774**	1.000**
NDVI	.069	.031	1.000**	1	.148	.157	-.731**	-.774**	1.000**
NDSI	-.117	-.285**	.148	.148	1	.964**	-.721**	-.643**	.138
SOCI	-.114	-.333**	.157	.157	.964**	1	-.730**	-.652**	.148
SWIR	.061	.243*	-.731**	-.731**	-.721**	-.730**	1	.993**	-.727**
SWIR2	.056	.231*	-.774**	-.774**	-.643**	-.652**	.993**	1	-.771**
Veg	.068	.027	1.000**	1.000**	.138	.148	-.727**	-.771**	1

Table 9. Multiple Linear Regression of Desert SOC and Spectral Indices; MLR model was developed using desert field-measured Soil Organic Carbon (SOC) as the dependent variable and various explanatory variables, including Landsat-9 spectral indices such as BI, RI, SAVI, SWIR2 BI2, CI, SOCI, SI, BSI, SWIR, Veg, RI, and NDVI.

Multiple Linear Regression of Desert SOC 2022						
Variables entered/ removed		**ANOVA**				
Entered	**Removed**		**Sum of Squares**	**df**	**Mean Square**	**F**
Veg, SI, BSI, CI, SWIR2, SOCI, SWIR, RI	SAVI, NDVI, BI2, NDSI, BI	Regression	2.329	8	.291	4.459
Model Summary		Residual	5.419	83	.065	
R	.548[a]	Total	7.748	91		
R^2	.301	**Model Coefficients**				
Adjusted R^2	.233		Unstandardized coefficients		Standardized coefficients	T
Std. Error	.255		B	Beta		
Model Equation: SOC = 43.35+ 14.421* BSI -242427.04* RI+113.68* CI-.291*SI+.001*SOCI+ 14.33SWIR-1.763*Veg		(Constant)	43.357	71.149		.609
		BSI	14.421	2.860	.517	5.043
		RI	-242427.048	299856.653	-3.049	-.808
		CI	113.687	184.565	1.635	.616
		SI	-.291	.464	-4.583	-.627
Dependent variable: SOC Predictors: (Constant), Veg, SI, BSI, CI, SWIR2, SOCI, SWIR, RI		SOCI	.001	.002	1.438	.423
		SWIR	14.337	27.985	1.630	.512
		SWIR2	.000	.001	-1.732	-.651
		Veg	-1.763	5.196	-.129	-.339

3.12. Spatial Mapping of SOC using MLR Model

Results showed that final iteration of the MLR model was employed to map the spatial distribution of SOC across the study area and the resultant output SOC spatial map is shown in Figure 8 and revealing distinct SOC patterns. MLR model illustrates elevated SOC levels (1.0 to 1.20) in the southern regions, including rangelands and barren lands, whereas a decline in SOC content (0.56 to 0.77) was noticeable in the northern parts of the study area. However, SOC range from 0.88 to 1.09 in the central parts of the study area. Compare to the results of IDW, the MLR model showed consistency in the northern and southern parts of the study area. Overall, model based on spectral indices computed from medium resolution (30 m) of Landsat-8 may be enhanced with high resolution satellite images specifically Synthetic Aperture Radar (SAR) data or fusion of high resolution optical and SAR data. Further, improved models of machine learning may also enhance SOC prediction particularly in desert areas.

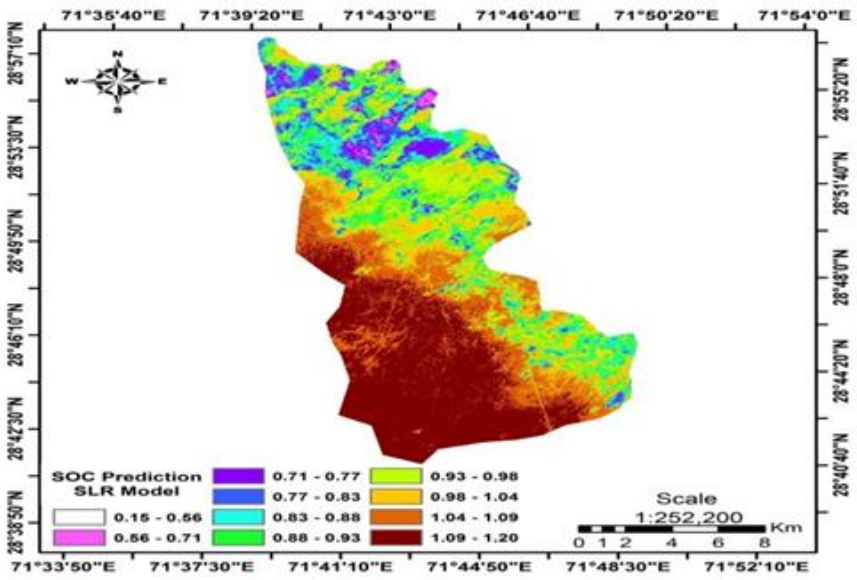

Fig. 8. Final iteration of the MLR model was employed to map the spatial distribution of SOC across the study area and the resultant output SOC spatial map.

SOC Interpolation by Inverse Distance Weightage Method

SOC of the desert has been interpolated through Inverse Distance Weightage (IDW) method and its resultant output map depicted in Figure 9. The results showed that the estimated SOC values ranged from 0.29 to 1.44, with an average of 0.89 which is consistent with mean observed SOC of 0.90. The standard deviation was 0.17, and the skewness coefficient was 0.36. Furthermore, the kurtosis coefficient for the predicted SOC values was calculated to be 0.66. Comparatively, the statistics of predicted SOC showed uniformity with that of observed SOC. An examination of the data distribution revealed a consistent pattern between the observed and estimated SOC, with a standard error of 0.018. The spatial pattern resulting from the IDW interpolation revealed an upward trend in SOC density (ranging from 0.93 to 1.42) moving towards southern parts of the study area. Conversely, lower SOC values (ranging from 0.74 to 0.88) were noted in the central parts. However, SOC levels near water bodies exhibited higher values, likely attributable to the presence of sparse vegetation.

As there was no dense vegetation in the desert area and only scattered trees/ fragmented shrubs were observed. Moreover, it has been revealed from the spectral indices computed from Landsat-9 images (of 30m resolution) that no prominent dense vegetation exist in the study area. Therefore biomass estimation in desert area was not possible based on the spectral information derived from medium resolution images of Landsat-9. However, data of biomass/ vegetation collected during field inventory have been explained. In order to quantify the tree specific biomas estimation, commercial satellite images upto spatial resolution of 0.5m or less required to mapping of scattered trees/ fragmented shrubs.

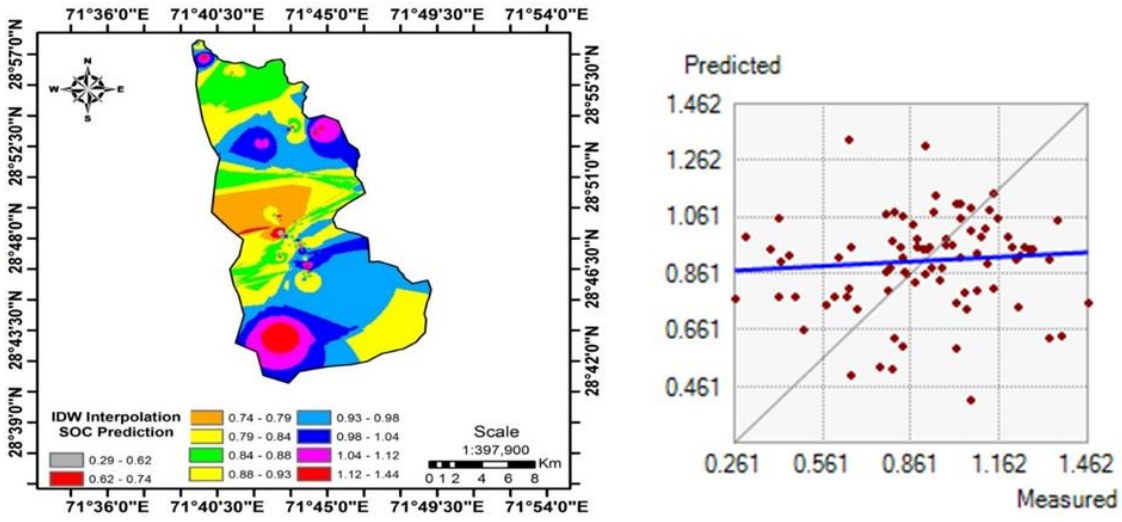

Fig. 9. IDW Interpolation SOC Prediction; SOC of the desert has been interpolated through Inverse Distance Weightage (IDW) method and its resultant output map.

4. Discussion

Natural ecosystems are the key source of above and below ground carbon and food source in the world (Vicharnakorn *et al*., 2014). Reduction in biological diversity always leads to the diminution of stored carbon stock that runs the natural ecosystems. Natural ecosystems are the key source of above and below ground carbon and food source in the world (Vicharnakorn *et al*., 2014). Reduction in biological diversity always leads to the diminution of stored carbon stock that run the natural ecosystems. Our study reveals that maximum amount of soil carbon was obtained in irrigated lands of Cholistan desert that was 2.125 in irrigated lands of desert and minimum was in sand dunes of lal-suhanra that was 1.260. Agricultural zones have more soil carbon than the desert because of land use and productivity (Srinivasarao *et al*., 3013). Desert type ecosystem always face the severe drought and temperature stress and cause soil deterioration that ultimately reduce the carbon storage in soil (Cusack *et al*., 2013; Lu *et al*., 2014).

Blaser *et al*., (2014) and Ludwig, *et al*., (2004) studied the effects of savannah vegetation and woody encroachment on soil organic carbon and soil nutrients. They studied that nitrogen fixation genus *vachellia* fix and store nitrogen in soil and found that soil organic matter is very consistent with the nitrogen stored in the soil due to vachellia genus. Our study sites have nitrogen fixation species i-e *vachellia nilotica, vachellia jacquemontii, prosopis juliflora* and *prosopis glandulus* and found the similar kind of results that different study sites have different soil carbon as studied by (Blaser *et al*., 2014; Ludwig *et al*., 2004).

Anwar *et al*., (2018) studied the biomass and carbon estimation of different tree species *Ziziphus jujuba, Acacia nilotica, Ficus palmate* and *Acacia modesta* and found that different species have different biomass, volume and carbon stock while our study reveals the similar kind of results in volume of *Vachellia nilotica* which is 3.286 m^3 in 2021 and 0.975 m^3 in 2022, *Ziziphus jujuba* which is 0.277 m^3 in 2021 and 1.164 m^3 in 2022, *Z. mauritiana* which is 17.34 m^3 in 2021 and 12.20 m^3 in 2022, Z. spine cristi which is 3.962 m^3 in 2021 and 2.432 m^3 in 2022, *Z. nummularia* which is 0.330 m^3 in 2021 and 0.243 m^3 in 2022 as shown in table 2. Our study also reveals that similar kind of results in biomass and carbon stock (Anwar *et al*., 2018).

Previously many researchers have found that variation in soil depth, vegetation structure, elevation and slope have different SOC contents (Bookhagen *et al*., 2005; Chan 2008; McGrath, and Zhang 2003). During the research we have found different SOC in ecosystem as CWLS and soil in LSNP. The study area LSNP and CWLS has 5 stratifications such as forest, agricultural land, sand dune, loamy and clay patch. Each site has different SOC contents Table 6 & 7, these results are similar to the findings of Bhunia *et al*., (2018) as they resulted different SOC in forest and agricultural areas. They also found different SOC at different soil depth 0 upto 20, 20 to 40 and 40 to 100 cm depth. We have found the similar results that different soil depth has different SOC. During the study OK, IDW were used for SOC interpolation. Both of there were good but IDW was found more accurate than the OK. Bhunia *et al*., (2018) has found the same results and said IDW interpolation is better than OK for SOC. They also discussed the results of (Varouchakis, and Hristopulos 2013; Venteris *et al*., 2014; Tripathi *et al*., 2015) that found that IDW interpolation is the best for SOC.

The current study includes the use of Landsat 9 and Landsat 8 spectral indices, the spectral indices included NDVI, SAVI, MSAVI, DVI and PVI. Pizana, *et al*., (2016) studied the remote sensing and geo-statistical techniques; used for vegetation and its biomass assessment. Coefficient of correlation for the MSAVI model (R^2 0.60) was lower than that of NDVI and SAVI, suggesting that this model explained around 60% of the biomass data, leaving 40% unexplained. In contrast, both DVI and PVI showed higher coefficient of correlation (R^2 0.67) compared to all other indices, indicating that they explained approximately 67% of the field biomass data, with about 33% remaining unexplained. Barati, *et al*., (2011) also studied the SAVI, MSAVI, NDVI, DVI and PVI for vegetation indices. Clerici, *et al*., (2016) also find the same results by using NDVI, PVI, DVI, SAVI and MSAVI. Ahmad, *et al*., (2023) also used SAVI, MSAVI and NDVI and found MLR method is best for correlation rather than the simple linear regression to estimate for biomass production.

5. Conclusion

This study provides valuable insights into the spatial distribution of soil organic carbon (SOC) in the study area highlighting the influence of land use patterns, vegetation indices, and interpolation methods on SOC estimation. By employing geostatistical techniques alongside remote sensing data, the research effectively mapped SOC variability across diverse land use types. The findings reveal that SOC levels are significantly influenced by proximity to water bodies, vegetation density, and land use type, with higher values near water bodies due to sparse vegetation. The study underscores the importance of integrating field sampling with remote sensing-derived vegetation indices to improve SOC prediction accuracy in arid and semi-arid regions. Additionally, the spatial distribution patterns observed through IDW and OK interpolation methods provide a foundational framework for identifying areas with high carbon storage potential. This information is critical for establishing carbon sink centers aimed at mitigating the adverse effects of climate change and global warming. This research not only advances our understanding of SOC dynamics in ecologically sensitive areas but also offers practical

applications for sustainable land management and climate change mitigation strategies. While Landsat data provided moderate-resolution insights, future work should consider incorporating higher-resolution data (e.g., Sentinel-2 at 10m or commercial imagery with sub-meter resolution) and advanced methods such as machine learning or radar-optical fusion to improve predictions in arid and sparsely vegetated landscapes.

Abbreviation

O=Ordinary Kriging
SOC =Soil Organic Carbon
IDW= Inverse distance weighting
LSNP= Lal Suhanra National Park
CWLS= Cholistan Wildlife Sanctuary
TC= Total Carbon
LULC= Land use land cover
BGB= Below Ground Biomass
AGB= Above Ground Biomass
V= Volume
WD= Wood Density
BEF= Biomass Expansion Factor

Declarations

Ethics approval and consent to participate

Conflict of interest: The Authors declared that they have no conflict of interest.

Data availability: Data will be available on demand.

Ethical approval: Not applicable.

Acknowledgement: Authors are highly acknowledged for their contribution.

Consent for publication: The article contains no such material that may be unlawful, defamatory, or which would, if published, in any way whatsoever, violate the terms and conditions as laid down in the agreement.

Funding detail: No funds available

Author's contribution: Muneeb Khalid, PhD scholar/researcher; Dr. Sanagam Khalil, supervisor; Conceptualization; Dr. Muhammad Abid, writing the manuscript; Prof. Dr. Tanveer Hussain, analyzing the data, Prof. dr. Muhammad Rafay, statistical analysis, Muhammad Madnee, review the article.

References

Abid, M., Rafay, M., Hussain, T., Sabir, M. A., Khalid, M., Madnee, M., ... & Iqbal, R. (2024). Salinity effects on growth, biomass production, and genetic resources for phytoremediation potential of halophyte species in the desert. *Genetic Resources and Crop Evolution*, 1-16.

Agarwal, C., G.M. Green and J.M. Grove. 2002. A review and assessment of land-use change models: dynamics of space, time, and human choice. In: Technical report, US Department of Agriculture, Forest Service, North- Eastern Research Station, Pennsylvania, USA.

Agrawal, O.P., K.V.G.K. Rao, H.S.Chauhan and M.K. Khandelwal. 1995. Geostatistical analysis of soil salinity improvement with subsurface drainage system. In: Transactions of ASAE 38, 1427–1433.

Ahmad, A., S.N. Mirza and S.M. Nizami. 2014. Assessment of biomass and carbon stocks in coniferous forest of Dir Kohistan, KPK. Pakistan Journal of Agricultural Sciences, 51(2).

Ahmad, N., S. Ullah, N. Zhao, F. Mumtaz, A. Ali, A. Ali, and M. Shakir. 2023. Comparative Analysis of Remote Sensing and Geo-Statistical Techniques to Quantify Forest Biomass. Forests, 14(2), 379.

Ali, A., M.I. Ashraf, S. Gulzar and M. Akmal. 2020. Development of an allometric model for biomass estimation of Pinus roxburghii, growing in subtropical pine forests of Khyber Pakhtunkhwa, Pakistan. Sarhad Journal of Agriculture, 36(1), 236-244.

Ali, A., M.I. Ashraf, S. Gulzar and M. Akmal. 2020. Development of an allometric model for biomass estimation of Pinus roxburghii, growing in subtropical pine forests of Khyber Pakhtunkhwa, Pakistan. Sarhad Journal of Agriculture, 36(1), 236-244.

Ali, A., S. Ullah, S. Bushra, N. Ahmad, A. Ali and M.A. Khan. 2018. Quantifying forest carbon stocks by integrating satellite images and forest inventory data. Austrian Journal of Forest Science/Centralblatt fur das gesamte Forstwesen, 135(2).

Barati, S., B. Rayegani, M Saati, A. Sharifi and M. Nasri. 2011. Comparison the accuracies of different spectral indices for estimation of vegetation cover fraction in sparse vegetated areas. The Egyptian Journal of Remote Sensing and Space Science, 14(1), 49-56.

Behera, S.K. and A.K. Shukla. 2015. Spatial distribution of surface soil acidity, electrical Conductivity, soil organic carbon content and exchangeable Potassium, calcium and magnesium in some cropped acid Soils of India. Land Degrad. Dev. 26, 71–79.

Bhunia, G. S., P.K. Shit and R. Maiti. 2018. Comparison of GIS-based interpolation methods for spatial distribution of soil organic carbon (SOC). Journal of the Saudi Society of Agricultural Sciences, 17(2), 114-126.

Blaser, W. J., G.K. Shanungu, P.J. Edwards, and H. Olde Venterink. 2014. Woody encroachment reduces nutrient limitation and promotes soil carbon sequestration. Ecology and evolution, 4(8), 1423-1438.

Bookhagen, B., R.C. Thiede, M.R. Strecker. 2005. Abnormal monsoon years and their control on erosion and sediment flux in the high, arid northwest Himalaya. Earth Planet. Sci. Lett. 231, 131–146.

Chan, Y. 2008. www.dpi.nsw.gov.au/primefacts.

Chung, H., J.H. Grove, J. Six, J. 2008. Indications for soil carbon saturation in a temperate agroecosystem. Soil Sci. Soc. Am. J. 72, 1132–1139.

Clerici, N., K. Rubiano, A. Abd-Elrahman, J.M. Posada Hoestettler, and F.J. Escobedo. 2016. Estimating aboveground biomass and carbon stocks in periurban Andean secondary forests using very high resolution imagery. Forests, 7(7), 138.

Cusack, D. F., O.A. Chadwick, T. Ladefoged, and P.M. Vitousek. 2013. Long-term effects of agriculture on soil carbon pools and carbon chemistry along a Hawaiian environmental gradient. Biogeochemistry, 112, 229-243.

Ekoungoulou, R., S. Niu, J.J. Loumeto, S.A. Ifo, Y.E. Bocko, F.E.K. Mikieleko, and X. Liu. 2015. Evaluating the carbon stock in above-and below-ground biomass in a moist central African forest. Applied Ecology and Environmental Sciences, 3(2), 51-59.

Elbasiouny, H., M. Abowaly, A. Abu Alkheir, A. Gad. 2014. Spatial variation of soil carbon and nitrogen pools by using ordinary Kriging method in an area of north Nile Delta, Egypt. Catena 113, 70–78.

Gogoi, N., Choudhury, M., Ul Hasan, M. S., Changmai, B., Baruah, D., & Samanta, P. (2024). Soil organic carbon pool in diverse land utilization patterns in North-East India: an implication for carbon sequestration. Environment, Development and Sustainability, 1-27.

Grass Biomass Production Above the Ground. 2023. https://www.climate-policy-watcher.org/carbon-stocks/grass-biomass-production-above-the-ground.html

Gregorich, E.G., M.R. Carter, D.A. Angers, C.M. Monreal, and B.H. Ellert. 1994. Toward minimum data set to assess soil organic matter quality in agricultural soils. Can. J. Soil Sci. 74, 885–901.

Greve, M.H., M.B. Greve, R. Bou Kheir, P.K. Bøcher, R. Larsen, and K. McCloy. 2009. Comparing decision tree modeling and indicator Kriging for mapping the extent of organic soils in Denmark. In: Boettinger, J.L., Howell, D.W., Moore, A.C., Hartemink, A.E., Kienast-Brown, S. (Eds.), Digital Soil Mapping Bridging Research, Environmental Application, and Operation. Springer, Dordrecht, Heidelberg, London, New York.

Guidelines for sensitive and critical areas, Govt. of Pakistan, Oct 1997.

Hameed, M., M. Ashraf, F. Al-Quriany, T.Nawaz, M. S. A. Ahmad, A. Younis and N. Naz. 2011. Medicinal flora of the Cholistan desert: a review. Pak. J. Bot 43(2): 39-50.

Hussain, I., M. Shakeel, M. Faisal, Z.A. Soomro, and T. Hussain. 2014. Distribution of total dissolved solids in drinking water by means of Bayesian kriging and gaussian spatial predictive process water quality. Expos. Health 6 (4), 177–185.

IPCC, 2003. Good Practice Guidance for Land Use, Land-Use Change and Forestry. The intergovernmental panel on climate (ipcc), Hayama, Japan.

Jobbagy, E.G., and R.B. Jackson. 2000. The vertical distribution of soil organic carbon and its relation to climate and vegetation. Ecol. Appl. 10, 423–436.

Johnston, K., J.M. Ver, Hoef K. Krivoruchko, and N. Lucas. 2001. Using ArcGIS Geostatistical Analyst. ESRI Press, Redlands, CA.

Kingsley, J., Afu, S. M., Isong, I. A., Chapman, P. A., Kebonye, N. M., & Ayito, E. O. (2021). Estimation of soil organic carbon distribution by geostatistical and deterministic interpolation methods: a case study of the southeastern soils of Nigeria. Environmental Engineering & Management Journal (EEMJ), (7).

Kumar, R., V.C. Pande, A.K. Bhardwaj, D. Dinesh, P.R. Bhatnagar, S. Dobhal, and K. Verma. 2022. Long-term impacts of afforestation on biomass production, carbon stock, and climate resilience in a degraded semi-arid ravine ecosystem of India. Ecological Engineering, 177, 106559.

Kumar, S., R. Lal, D. Liu, and R. Rafiq. 2013. Estimating the spatial distribution of organic carbon density for the soils of Ohio, USA. J. Geogr. Sci. 23 (2), 280–296.

Kumar, S., R. Lal, D.C. Lloyd. 2012. Assessing spatial variability in soil characteristics with geographically weighted principal components analysis. Comput. Geosci. 16, 827–835. http://dx.doi.org/ 10.1007/s10596-012-9290-6.

Lambin E.F., B.L. Turner H.J. Geist. 2001. The causes of land-use and land cover change: Moving beyond the myths. In: Global Environmental Change, vol. 11(4), pp. 261-269.

Liu, L., H. Wang, W. Dai, X. Lei, X., Yang, X., Li. 2014. Spatial variability of soil organic carbon in the forestlands of northeast China. J. Forest. Res. 25 (4), 867–876.

Lu, D., P. Mausel E. Brondizio. 2004. Change detection techniques. In: International Journal of Remote Sensing, vol. 25(12), pp. 2365-2407.

Lu, Y., Z. Ma, Z. Zhao, F. Sun, and B. Fu. 2014. Effects of land use change on soil carbon storage and water consumption in an oasis-desert ecotone. Environmental management, 53, 1066-1076.

Ludwig, F., H. de Kroon, F. Berendse, and H.H.T. Prins. 2004. The influence of savanna trees on nutrient, water and light availability and the understory vegetation. Plant Ecology 170, 93–105, https://doi.org/10.1023/B:VEGE.0000019023.29636.92.

Luo, Z., E. Wang, O.J. Sun. 2010. Soil carbon change and its responses to agricultural practices in Australian agro-ecosystems: a review and synthesis. Geoderma 155, 211–223.

Magar, L.K., G. Kafle, and P. Aryal. 2020. Assessment of soil organic carbon in tropical agroforests in the Churiya Range of Makawanpur, Nepal. International Journal of Forestry Research, 2020, 1-5.

Mallupattu, P.K., J. Reddy S. Reddy. 2013. Analysis of land use/land cover changes using remote sensing data and GIS at an urban area, Tirupati, India. In: The Scientific World Journal, vol. 2013(6), article no. 268623.

Margono, B. A., S. Turubanova, I. Zhuravleva, P. Potapov, A. Tyukavina, A. Baccini and M.C. Hansen. 2012. Mapping and monitoring deforestation and forest degradation in Sumatra (Indonesia) using Landsat time series data sets from 1990 to 2010. Environmental Research Letters 7(3): 034010.

McGrath, D., C. Zhang. 2003. Spatial distribution of soil organic carbon concentrations in grassland of Ireland. Appl. Geochem. 18 (10), 1629–1639.

Mirzaei, R., M. Sakizadeh. 2015. Comparison of interpolation methods for the estimation of groundwater contamination in Andimeshk–Shush Plain Southwest of Iran. Environ. Sci. Pollut. Res., 1–12.

Mondal, A., D. Khare, S. Kundu, S. Mondal, S. Mukherjee, and A. Mukhopadhyay. 2017. Spatial soil organic carbon (SOC) prediction by regression kriging using remote sensing data. The Egyptian Journal of Remote Sensing and Space Science, 20(1), 61-70.

Nabi, K., K. Ali, M.I. Ashraf, A.B. Imran, and N. Ahmad. 2021. Assessment of land cover changes due to anthropogenic causes in the mountainous area of Ishkoman Watershed, Gilgit, Pakistan. Bulletin of the Transilvania University of Brasov. Series II: Forestry• Wood Industry Agricultural Food Engineering, 25-46.

Nizami, S.M., S.N. Mirza, S. Livesley, S. Arndt, J.C Fox, I.A. Khan, and T. Mahmood. 2009. Estimating carbon stocks in sub-tropical pine (Pinus roxburghii) forests of Pakistan. Pakistan Journal of Agricultural Sciences, 46(4), 266-270.

Pang, S., T.X.Li, X.F. Zhang, Y.D. Wang, H.Y. Yu. 2011. Spatial variability of cropland lead and its influencing factors: a case study in Shuangliu county, Sichuan province, China. Geoderma 162, 223–230.

Patel, R., Sharief, S., Kodchire, A., & Panwar, V. P. (2024). Predicting Soil Organic Carbon in Forest Soils of Telangana, India: A Comparative Analysis of Deterministic and Geostatistical Interpolation Models. Journal of Soil Science and Plant Nutrition, 24(4), 7853-7868.

Pizana, J. M. G., J.M.N. Hernández, and N.C. Romero. 2016. Remote sensing-based biomass estimation. Environmental Applications of Remote Sensing.

Qi J., A.L. Chehbouni, A.R. Huete, Y.H. Kerr and S. Sorooshian. 1994. A modified soil adjusted vegetation index (MSAVI). Remote Sensing of Environment48: 119-126.

Raheem, A. M., Naser, I. J., Ibrahim, M. O., & Omar, N. Q. (2023). Inverse distance weighted (IDW) and kriging approaches integrated with linear single and multi-regression models to assess particular physico-consolidation soil properties for Kirkuk city. Modeling earth Systems and environment, 9(4), 3999-4021.

Robertson, G.P., 2008. GS+: Geostatistics for the Environmental Sciences. Gamma Design, Plainwell, Mich.

Robinson, T.P., and G.M. Metternicht. 2006. Testing the performance of spatial interpolation techniques for mapping soil properties. Comput. Electeron. Agric. 50, 97–108.

Sahu, B., & Ghosh, A. K. (2021). Deterministic and geostatistical models for predicting soil organic carbon in a 60 ha farm on Inceptisol in Varanasi, India. Geoderma Regional, 26, e00413.

Saito, H., A. McKenna, D.A. Zimmerman, T.C. Coburn. 2005. Geostatistical interpolation of object counts collected from multiple strip transects: ordinary kriging versus finite domain kriging. Stoch. Environ. Res. Risk Assess. 19, 71–85.

Srinivasarao, C., B. Venkateswarlu, R. Lal, A.K. Singh, and S. Kundu. 2013. Sustainable management of soils of dryland ecosystems of India for enhancing agronomic productivity and sequestering carbon. Advances in agronomy, 121, 253-329.

Stevenson, F.J., Cole, M.A., 1999. Cycles of Soil, second ed. Wiley, New York.

Tripathi, R., A.K. Nayak, M. Shahid, R. Raja, B.B. Panda, S. Mohanty, and R.N. Sahoo. 2015. Characterizing spatial variability of soil properties in salt affected coastal India using geostatistics and kriging. Arabian Journal of Geosciences, 8, 10693-10703.

United States Department of Agriculture-Natural Resources Conservation Service (USDA-NRCS), 1995. Soil Survey Laboratory Information Manual. Soil Survey Investigations Report No. 45. National Soil Survey Center, Soil Survey Laboratory, Lincoln, Nebraska.

Varouchakis, E. A., and D.T. Hristopulos. 2013. Comparison of stochastic and deterministic methods for mapping groundwater level spatial variability in sparsely monitored basins. Environmental monitoring and assessment, 185, 1-19.

Vauclin, M., S.R. Vieira, G. Vachaud, and D.R. Nielsen. 1983. The use of cokriging with limited field soil observations. Soil Sci. Soc. Am. J. 47, 175–184.

Venteris, E. R., N.T. Basta, J.M. Bigham, and R. Rea. 2014. Modeling spatial patterns in soil arsenic to estimate natural baseline concentrations. Journal of environmental quality, 43(3), 936-946.

Vicharnakorn, P., R.P. Shrestha, M. Nagai, A.P. Salam and S. Kiratiprayoon. 2014. Carbon stock assessment using remote sensing and forest inventory data in Savannakhet, Lao PDR. Remote Sensing 6(6): 5452-5479.

Wariss, H. M., S.A. Pirzada, K. Alam, S. Anjum and R. Qureshi. 2014. Flora of LalSuhanra National Park, Bahawalpur, Punjab, Pakistan. Pak. J. Bot, 46(4): 1331-1341.

Wei, J.B., D.N. Xiao, H. Zeng, Y.K Fu. 2008. Spatial variability of soil properties in relation to land use and topography in a typical small watershed of the black soil region, northeastern China. Environ. Geol. 53, 1663–1672.

Wu, J., and R. Hobbs. 2002. Key issues and research priorities in landscape ecology: An idiosyncratic synthesis. In: Landscape Ecology, vol. 17, pp. 355-365.

Zare-mehrjardi, M., R. Taghizadeh-Mehrjardi, A. Akbarzadeh. 2010. Evaluation of geostatistical techniques for mapping spatial distribution of soil PH, salinity and plant cover affected by environmental factors in Southern Iran. Not. Sci. Biol. 2 (4), 92–103.

Zhang, W., K.L. Wang, H.S. Chen, X.Y. He, and J.G. Zhang. 2012. Ancillary information improves kriging on soil organic carbon data for a typical karst peak cluster depression landscape. J. Sci. Food Agric. 92 (5), 1094–1102.

Zhao, G.X., G. Lin and T. Warner. 2004. Using thematic mapper data for change detection and sustainable use of cultivated land: A case study in the Yellow River delta, China. In: International Journal of Remote Sensing, vol. 25(13), pp. 2509-

Zhu, C., Wei, Y., Zhu, F., Lu, W., Fang, Z., Li, Z., & Pan, J. (2022). Digital mapping of soil organic carbon based on machine learning and regression kriging. Sensors, 22(22), 8997.